

Fragment-Based Discovery of Bromodomain Inhibitors Part 2: Optimization of Phenylisoxazole Sulfonamides

Paul Bamborough,^{*,‡,||} Hawa Diallo,[†] Jonathan D. Goodacre,[†] Laurie Gordon,[§] Antonia Lewis,[§] Jonathan T. Seal,[†] David M. Wilson,[†] Michael D. Woodrow,[†] and Chun-wa Chung^{‡,||}

[†]Epinova DPU, Immuno-Inflammation Centre of Excellence for Drug Discovery, GlaxoSmithKline R&D, Medicines Research Centre, Gunnels Wood Road, Stevenage, Hertfordshire SG1 2NY, U.K.

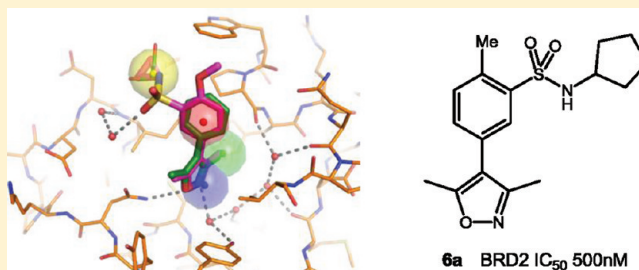
[‡]Computational & Structural Chemistry, Molecular Discovery Research, GlaxoSmithKline R&D, Medicines Research Centre, Gunnels Wood Road, Stevenage, Hertfordshire SG1 2NY, U.K.

[§]Screening & Compound Profiling, Molecular Discovery Research, GlaxoSmithKline R&D, Medicines Research Centre, Gunnels Wood Road, Stevenage, Hertfordshire SG1 2NY, U.K.

S Supporting Information

ABSTRACT: Bromodomains are epigenetic reader modules that regulate gene transcription through their recognition of acetyl-lysine modified histone tails. Inhibitors of this protein–protein interaction have the potential to modulate multiple diseases as demonstrated by the profound anti-inflammatory and antiproliferative effects of a recently disclosed class of BET compounds. While these compounds were discovered using phenotypic assays, here we present a highly efficient alternative approach to find new chemical templates, exploiting the abundant structural knowledge that exists for this target class.

A phenyl dimethyl isoxazole chemotype resulting from a focused fragment screen has been rapidly optimized through structure-based design, leading to a sulfonamide series showing anti-inflammatory activity in cellular assays. This proof-of-principle experiment demonstrates the tractability of the BET family and bromodomain target class to fragment-based hit discovery and structure-based lead optimization.



■ INTRODUCTION

Bromodomain (BD) modules regulate the structure of chromatin, and thereby gene expression, through their ability to “read” the acetylated-lysine state of histone tails.¹ Bromodomain-containing proteins (BCPs) have been associated with numerous conditions including diabetes, obesity, oncology, inflammation, viral infection, metabolic, and cardiovascular disorders.^{1–4} The discovery of the first potent bromodomain inhibitors using cellular phenotypic assays has recently been reported.^{5,6} These benzodiazepines (BZDs, Table 1) target the BET family (BRD2, BRD3, BRD4) tandem bromodomains,⁴ which showed for the first time that the BET/histone protein–protein interaction can be disrupted by small molecules. In an accompanying paper,⁷ we demonstrate that this interaction can also be blocked by fragment-sized molecules selected to target the “hotspot” of the acetyl-lysine (AcK) pocket. Crystallography confirmed that these chemically diverse fragments exhibit remarkably similar binding features within this recognition site.

Fragment-based drug discovery (FBDD) uses high-concentration screening to identify low-MW hits⁸ which, although weak, are efficient in terms of their binding energy per heavy atom, usually expressed as ligand efficiency or LE.⁹ Care must be taken to ensure that the attractive drug-like properties of the

fragments are not lost during optimization. For this, the binding pocket must be large and deep enough to allow elaboration that gains additional productive interactions. Iterative high resolution crystallography of protein–ligand complexes and molecular modeling predictions greatly assist the process of FBDD optimization. Structures of many bromodomains have now been solved, from which it appears that some have AcK pockets which may indeed be suitable for productive fragment growth. Here we describe how a structure-derived 3D pharmacophore was key to the rapid optimization of a weak BET fragment into compounds with cellular anti-inflammatory activity.

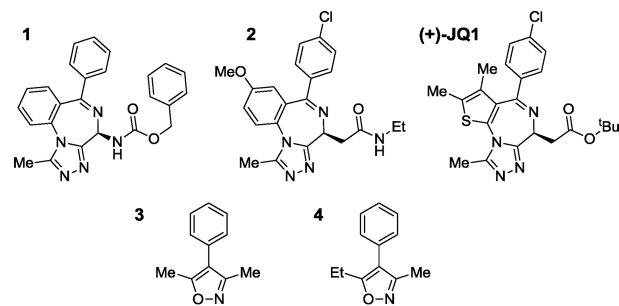
■ RESULTS

Fragment Screening. Initial screening was performed with a fluorescence anisotropy (FA) assay against the three tandem BET bromodomain constructs using a rationally selected screening set targeting the bromodomain AcK pocket. Numerous potential starting points were found, some of which are described elsewhere.⁷ 4-Phenyl 3,5-dimethyl isoxazole 3 was one of the hits (Table 1), showing activity of 32% and 26%

Received: August 23, 2011

Published: December 5, 2011

Table 1. Literature BET Bromodomain Inhibitors and Their Tandem Bromodomain IC₅₀ (μM, Mean of ≥7 Values) in FA, TR-FRET, and Isothermal Titration Calorimetry Assays^a



	FA (IC ₅₀ nM)			TR-FRET (IC ₅₀ nM)			ITC (Kd, nM)		
	BRD2	BRD3	BRD4	BRD2	BRD3	BRD4	BRD2	BRD3	BRD4
1	820	350	470	160	220	140	52	19	24
LE	.26	.28	.27	.29	.28	.29			
2	810	390	740	150	160	190	101	89	49
LE	.28	.29	.28	.31	.31	.31			

^aLigand efficiency (LE) calculated as $1.37(\text{pIC}_{50}/\text{number of heavy atoms})$ is also shown. (+)-JQ1 had IC₅₀ of 77 nM and 33 nM against isolated N- and C-terminal BRD4 bromodomains in a luminescence proximity homogeneous assay.⁶

at 200 μM against BRD3 and BRD4, respectively. While this was far from the most potent fragment detected, it was small, efficient, novel, and chemically attractive. It was also one of the fragments which is less directly related to acetyl-lysine. We therefore investigated its binding mode in order to optimize the potency of the series.

Crystal Structure of Phenyl Isoxazole Fragment 3.

Compounds have previously been shown to bind with similar affinity and identical binding mode to both N- and C-terminal bromodomains of the highly homologous BET family members.¹⁰ Therefore we used X-ray structures of compounds soaked into apo crystals of the N-terminal bromodomain of BRD2 (BRD2-BD1) to exemplify their interactions within the AcK pocket⁷ (Supporting Information Figure S1). The C2 crystal form contains 3 molecules in the asymmetric unit (ASU) whose AcK pockets are differentially accessible (chains A–C, Figure 1A).

The dimethyl isoxazole 3 binds in accord with the hypothesis underlying the focused set selection.⁷ One of the two methyl groups of the dimethyl isoxazole occupies the small pocket adjacent to Phe99, mimicking the terminal methyl of the AcK side chain (Figure 1B,C, Figure 2A). The second methyl group overlays with the ε-CH₂ group of the AcK side chain, contacting the side chain of Leu110. The isoxazole nitrogen and oxygen atoms together mimic the AcK carbonyl group whose position is roughly midway between the two (Figure 1B). Because the isoxazole ring is almost symmetrical, even at <2.0 Å resolution the electron density cannot differentiate the isoxazole heteroatoms unambiguously. The true binding mode of 3 may be one in which the nitrogen and oxygen exchange positions or inhibition may result from a mixture of both binding modes if the energy difference is small.

This uncertainty cannot be resolved by the observed interactions: both heteroatoms are roughly equidistant (2.7–2.9 Å) from a water molecule that is itself hydrogen-bonded to the side chain oxygen of Tyr113. This bridging water molecule is one of the most highly conserved in BRD2/fragment crystal

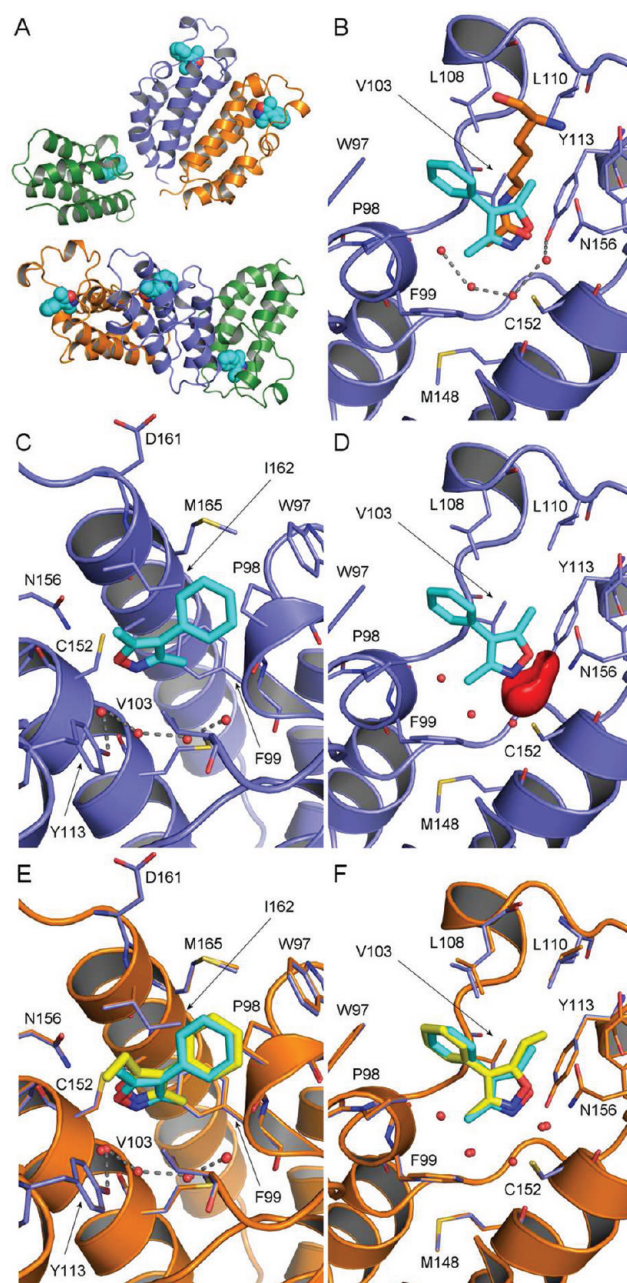


Figure 1. (A) The ASU of BRD2-BD1 showing 3 (cyan) bound into chains A (blue), B (orange), and C (green), in two orientations: that of (B) above, and of (C) below. (B) Chain A (blue) and 3 (cyan), with the side chain of AcK (orange) taken from histone H4 1–20, K5Ac K8Ac bound to mouse BRDT (PDB 2wp2).²⁴ (C) As (B), in an alternative orientation. (D) As (B), showing the red electrostatic isopotential surface of 3. (E) The complex of 4 (yellow) in BRD2 (orange) with 3 (cyan), in the orientation of (C). (F) As (E), in the orientation of (B).

structures.⁷ For each heteroatom, the angle of interaction with the water deviates by over 50° compared to an ideal sp² lone pair. One of the heteroatoms is 3.2 Å away from the conserved AcK-binding side chain nitrogen of Asn156, but this is also 50° away from ideality. The isoxazole has been modeled so that the more electron-rich nitrogen atom is nearest to the water molecule (Figure 1D), in accord with our finding that for most fragments the ligand lies closer to the water than to Asn156.⁷ To attempt to confirm this, the 5-ethyl 3-methyl fragment 4

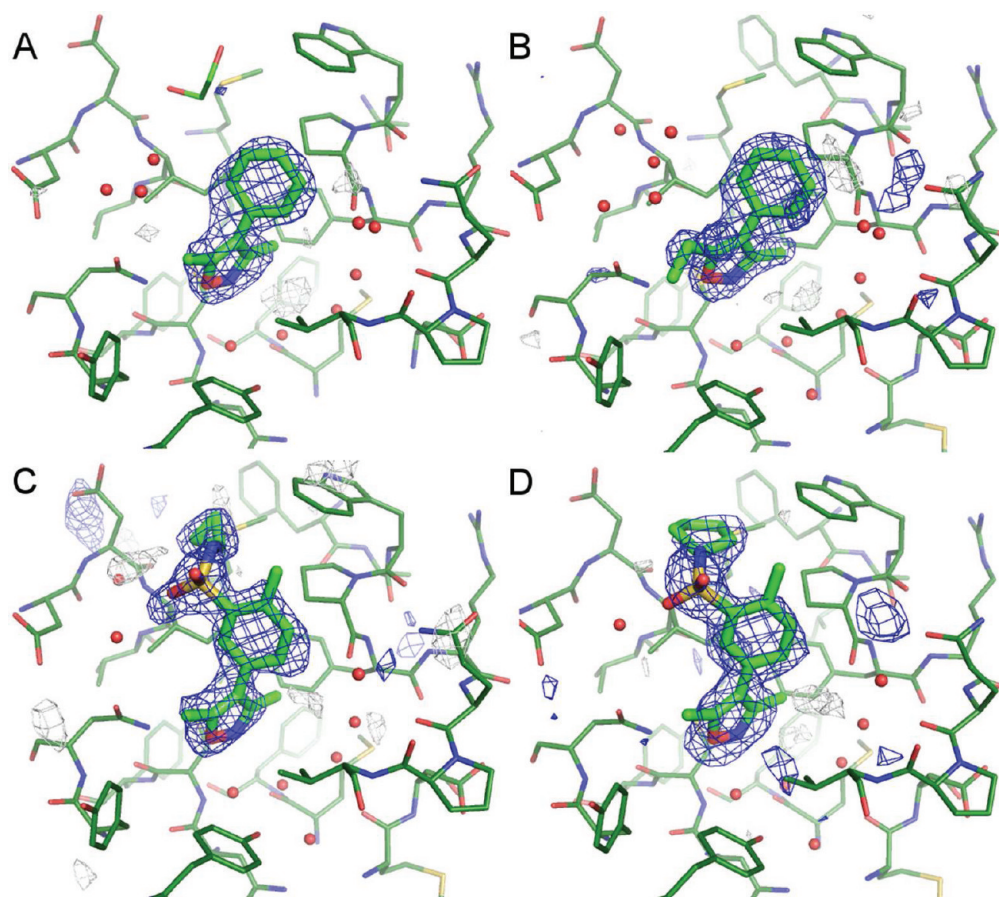


Figure 2. OMIT ($F_o - F_c$) difference maps of BRD2-BD1 complexes. (A) Complex with 3; (B) complex with 4; (C) complex with 5a; (D) complex with 6a. Contours are blue = 3σ , gray = -3σ for (A–C) and blue = 2σ , gray = -2σ for (D).

was synthesized and crystallized with BRD2-BD1. As the longer ethyl group is visible within the electron density, the binding mode of this compound can be determined with certainty, supporting the proposed orientation of the isoxazole in 3 (Figure 1E,F).

The phenyl ring of 3 occupies a tight cleft, sandwiched on either face by the aliphatic side chains of Pro98 and Leu108 (Figure 1B). The phenyl–isoxazole torsion angle varies between 51° and 59° for the three ligands in the asymmetric unit. While slightly greater than the quantum mechanics gas-phase minimized torsion of 44° (see Experimental Section), the calculated ΔE is negligible.

Initial Optimization. To find active analogues, our knowledge base of BET X-ray complexes was exploited using a variety of computational approaches. One method used 3D pharmacophore models to describe the essentials of the binding site. Steric and electrostatic features of the AcK headgroup were encapsulated by features placed upon critical atoms of the dimethyl isoxazole 3 (Figure 3A). Another key interaction was with the WPF shelf, a lipophilic region named after the sequence of residues 97–99 in BRD2, which we previously showed to bind aromatic rings of 1 and 2.¹⁰ Further, in the complex with 3, this site was occupied by ethylene glycol. Therefore a lipophilic feature was added to the pharmacophore at the centroid of the pendant phenyl ring of 1 (Figure 3A). The pharmacophore was used to search a database of commercially available compounds. Among the search hits was a cluster of phenyl isoxazole analogues of 3 with sulfonamide

substituents on the phenyl ring *meta* to the isoxazole. When fitted to the pharmacophore model, the sulfonamide introduces a bend into the shape of the molecule that causes the substituent to project in the direction of the WPF shelf (Figure 3B). Docking also predicted this binding mode, providing some validation for this hypothesis. Selected compounds were purchased and screened in dose–response mode, the results of which are shown in Table 2 and Supporting Information Figure S2. These compounds showed encouraging potency in both FA and TR-FRET assays, with IC_{50} in the low micromolar range. Compared to the fragment hit 3, which has an IC_{50} of above $200 \mu M$, 5a is at least 100-fold more potent. This was particularly interesting because IC_{50} s from the FA and TR-FRET assays can underestimate equilibrium affinities obtained from direct binding methods such as isothermal titration calorimetry due to the low tight binding limit of these competition assays (Table 1). The ligand efficiency (LE, approximated as $1.37(pIC_{50}/\text{number of heavy atoms})^9$) of 5a is 0.39, comparable to 3 based on $IC_{50} \approx 200 \mu M$, and superior to 1 and 2 (Table 1).

Crystal Structures of Optimized Sulfonamides. Examples of the sulfonamide series were soaked into crystals of BRD2-BD1. In the crystal form used, the Z-helix of chain A, especially its N-terminus around Asn77, is in close proximity to the AcK pocket of chain C,⁷ reducing the accessibility of this site (Figure 1A). Because of this, the AcK site of chain C in the complex with 5a is occupied by a DMSO molecule. The orientation of DMSO in chain C is very similar to that in

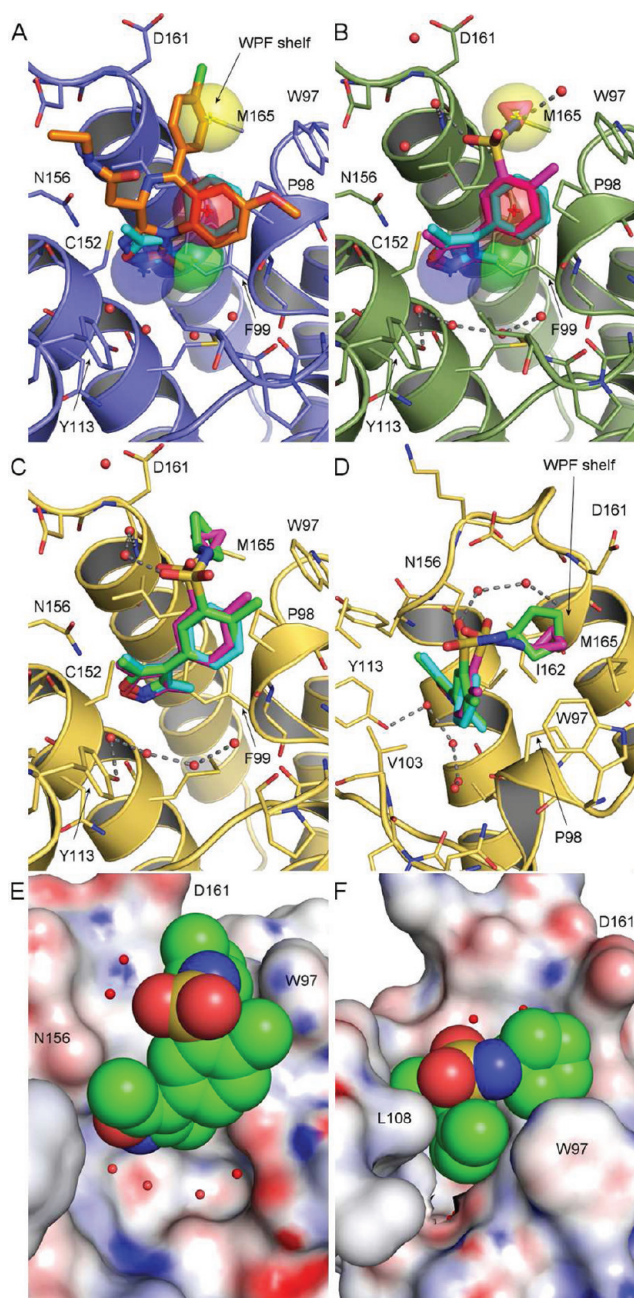


Figure 3. (A) The complex of BRD2 with **3** (cyan), with **2** (orange) superimposed in the orientation of Figure 1B. Transparent spheres represent pharmacophore features: blue = H-bond acceptor (AcK carbonyl); green = methyl; red = aromatic; yellow = lipophilic (WPF shelf). (B) BRD2 (olive) in complex with **5a** (magenta), superimposed on **3** (cyan). (C) BRD2 (yellow) in complex with **6a** (green), overlaid on **3** (cyan) and **5a** (magenta). (D) As (C), in alternative orientation looking down the phenyl/isoxazole bond. (E) BRD2 electrostatic potential surface with **6a** (spheres) in orientation of (C). (F) As (E) in orientation of (D).

CREBBP (PDB entry 3p1e)¹¹ and so will not be discussed further. In the more accessible A and B chains of the ASU, **5a** binds in an identical manner and as intended by the modeling hypothesis.

Figures 3B and 2 show the binding mode of **5a** in chain B, highlighting the similarity between its binding mode and that of fragment **3**. The isoxazole oxygen of **5a** lies within hydrogen-bonding distance of both Asn156 and the bridging water

molecule, and one of the two methyl groups fits into the methyl pocket. The sulfonamide substituent can be accommodated without the need for any change in the binding mode of the fragment or the interactions that it makes with the acetyl lysine pocket. The torsion angles between the isoxazole and phenyl rings are similar to those of **3** (51–56° in both chains). As predicted, the sulfonamide introduces a bend in the shape of the molecule that directs the cyclopropyl ring onto the WPF shelf, occupying the space of the lipophilic pharmacophore feature. It makes contact with the hydrophobic parts of the shelf, most extensively with the side chains of residues Trp97, Pro98, Ile162, and Met165, and the methylene group of the Asp161 side chain. The sulfonamide itself makes no direct hydrogen-bonding interactions with the protein but does participate in some water-mediated interactions. One of the sulfonamide oxygen atoms is close to a well resolved water molecule that caps the N-terminus of the α C-helix by hydrogen-bonding to the backbone NH of Ile162. An equivalent water molecule is also present in the complex with **3** and was always present in 40 crystal structures of BRD2-BD1 with various AcK-site fragments.⁷ The other oxygen and the nitrogen atom of the sulfonamide group are also close to water molecules, but the details vary from one molecule of the asymmetric unit to another so we do not believe that these interactions contribute strongly to binding.

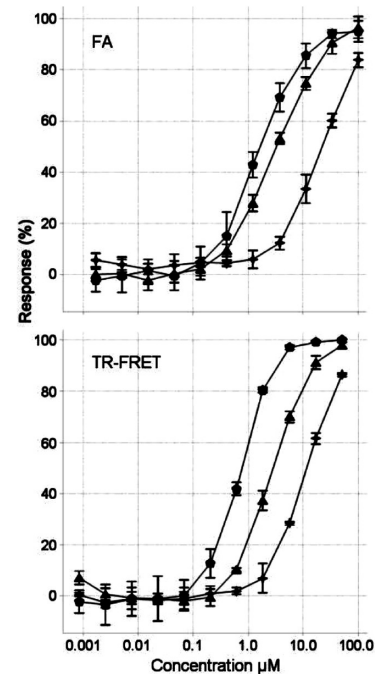
Structure–Activity Relationships. Expanding the cyclopropyl ring to cyclopentyl (**6a**, **6b**) and cyclohexyl (**7a**) gave compounds with increased activity but with a trend for decreasing ligand efficiency when normalized for the additional atoms introduced (Table 2). This suggests that the optimal size of the lipophilic substituent that can be accommodated by the WPF shelf is 3–5 heavy atoms. The cyclopentyl analogue **6a** binds to all three molecules of the ASU of the crystal (Figure 2). Compared to its position in chains A and B, the ligand moves slightly in chain C, probably as a result of the obstructed nature of this AcK site. Overall, the binding mode of the cyclopentyl **6a** in chains A and B is very similar to that of the cyclopropyl **5a** (Figure 3C,D). As with **5a**, the sulfonamide substituent of **6a** occupies the WPF shelf. The phenyl/isoxazole bond in the cyclopentyl structure is slightly more in-plane (37–43°) than in fragment **3** and the cyclopropyl **5a**, resulting in the C3 atom of the cyclopentyl ring overlaying almost perfectly with the C2 atom of the cyclopropyl sulfonamide (Figure 3D). Presumably this is because of steric contacts which prevent the cyclopropyl ring from moving any deeper into the pocket (Figure 3E,F). This rotation also results in a shift of the positions of the two sulfonamide oxygen atoms by about 1 Å, leading to subtle changes in the way that they coordinate water molecules. For example, one S=O group moves away from the α C-helix Ile162 capping water, so that the H-bonding interaction takes place through an extra intervening water molecule (compare parts B and C of Figure 3).

Even larger sulfonamide substituents, such as those of the phenyl-substituted **8a** and **8b**, are accommodated but are not optimal, as indicated by their decreased potency and LE (Table 2). Substitution on the phenyl ring at any position lowered the affinity, regardless of electronic accepting or donating ability (**9a–14a**, **9b–14b**), which can also be rationalized sterically. Our expectation was that the introduction of a chain linking the sulfonamide to the phenyl ring would be detrimental to binding because this would make it difficult for the phenyl ring to lie upon the WPF shelf and would increase the entropic penalty to binding. This was found to be the case for the benzyl-substituted

Table 2. (A) Activity of Sulfonamide Analogues against BRD2, BRD3, and BRD4 (TR-FRET Assay, μM) (See Supporting Information Figure S2 for Complete Data Including n and Standard Deviation; LE = Ligand Efficiency, $\Delta\text{G} \sim 1.37(\text{pIC}_{50}/N$ heavy atoms)); (B) Binding Curves of 5a (Triangles), 6a (Pentagons), and 29a (Crosses) in BRD4 FA and TR-FRET Assays

		a: R ₁ = Methyl							b: R ₁ = Methoxy							
		Mean IC ₅₀			LE				Mean IC ₅₀			LE				
R ₂	n	BRD2	BRD3	BRD4	BRD2	BRD3	BRD4	IL-6	BRD2	BRD3	BRD4	BRD2	BRD3	BRD4	IL-6	
	n=1	5	1.5	1.0	1.0	.38	.39	.39	3.3	1.9	1.3	3.0	.35	.37	.34	3.4
	n=3	6	0.5	0.5	0.6	.38	.38	.38	3.1	1.4	1.0	2.2	.34	.34	.33	1.2
	n=4	7	0.9	0.7	1.1	.34	.35	.34	4.1							
	X = H	8	1.1	1.0	1.8	.34	.34	.33	14	2.4	2.2	5.6	.31	.31	.29	8.4
	X = 2-Cl	9	1.8	2.0	3.0	.31	.31	.30		4.3	4.8	7.6	.28	.28	.27	
	X = 3-Cl	10	2.5	1.9	3.3	.31	.31	.30								
	X = 4-Cl	11	3.6	4.0	4.5	.30	.30	.30								
	X = 2-OMe	12	1.5	2.1	2.8	.31	.30	.30		4.9	5.4	8.2	.27	.27	.26	
	X = 3-OMe	13	2.0	1.9	2.6	.30	.30	.30		5.2	4.7	6.0	.27	.27	.26	
	n=1	15	4.7	3.8	6.6	.29	.30	.28		13	14	20	.26	.26	.25	
	n=2	16	4.4	3.3	4.4	.28	.29	.28								
	n=3	17	3.9	3.0	3.3	.27	.28	.28								
	X = (CH ₂) ₂ OMe	18	12	8.6	13	.31	.32	.31								
	X = (CH ₂) ₃ OH	19	5.6	4.2	6.5	.32	.34	.32								
	X = C(CH ₃) ₃	20	2.5	1.8	2.0	.35	.35	.35	5.9							
	X = H	21	8.1	8.6	7.4	.39	.39	.39								
	X = Et	22	2.2	1.5	2.4	.39	.40	.38	7.2							
	X = Me	23							0.8	0.7	1.0	.33	.34	.33	1.5	
	X = Et	24							0.8	0.7	1.3	.32	.33	.31	3.3	
	n=1 X=CH ₂	25	1.7	1.1	1.8	.36	.37	.36	2.5							
	n=2 X=CH ₂	26	1.1	0.8	1.2	.36	.36	.35	3.3							
	n=2 X=NH	27	14	8.2	12	.29	.30	.29	22	16	11	17	.27	.28	.27	29
	n=2 X=O	28	4.2	3.2	4.2	.32	.33	.32	4.4	11	6.5	11	.29	.30	.29	18
	X=CH ₂ Y=NH	29	19	11	15	.27	.29	.27	18	31	21	22	.25	.26	.26	55
	X=NH Y=CH ₂	30	11	8.4	10	.29	.29	.29		9.0	13	17	.27	.27	.26	

B



compounds (15a, 15b) and compounds with longer linking chains (16a, 17a). Similar arguments rationalize the reduced affinity of flexible straight-chain sulfonamides (18a, 19a), although the bulky *t*-butyl group of 20a appears sufficiently rigid and lipophilic to regain some of the loss.

For comparison, we synthesized the unsubstituted and ethyl sulfonamides 21a and 22a. Although the ethyl is slightly less potent than the cyclopropyl 5a and the unsubstituted sulfonamide is almost 10-fold less potent, they are of comparable efficiency. The water-mediated interactions of the sulfonamide described earlier, and potential additional water-mediated interactions of the primary sulfonamide might account for the improved activity of 21a over 3. Alkylation of the sulfonamide nitrogen was tolerated with marginally increased potency (23b, 24b) but with a slight decrease in efficiency. This is consistent with our belief that the water molecule seen near the sulfonamide nitrogen in the crystal structures of 5a and 6a is weakly bound. It also proved possible to homologate the nitrogen into the ring, producing the piperidine 25a and piperazine 26a. However, these compounds offered no clear advantage over the secondary sulfonamides and were slightly lower in ligand efficiency.

Improvement in Solubility. Low solubility was a limitation of the series (Table 3). To improve this, charge and polarity were incorporated at positions guided by the X-ray structures. As the WPF shelf is mainly lipophilic, we were concerned that introducing these properties into the sulfonamide

Table 3. Activity (TR-FRET and PBMC-IL6 Assays) and Solubility of Sulfonamide Analogues 31–34

	Mean IC ₅₀ (μM)				Solubility $\mu\text{g}/\text{ml}$	
	BRD2	BRD3	BRD4	IL-6	pH 5.0	pH 7.0
6a	0.5	0.5	0.5	3.1	< 1	< 1
25a	1.7	1.1	1.8	2.5	4	5
31	3.6	3.0	3.2			
32	1.5	1.4	2.5			
33	3.6	2.2	5.2	3.3	620	540
34	1.5	1.1	2.6	3.0	1125	210

substituent would be detrimental to binding (see electrostatic potential map, Figure 3E, Figure 3F). This was found to be the case because the introduction of polar groups led to reduced potency (for example 27a–30a, 27b–30b). Consequently, we turned to modifications of the phenyl ring *para* to the isoxazole. Diversity at this position in the commercially available compounds was restricted to methyl and methoxy. This position

points toward the solvent (Figure 2C), and there was little difference in potency between the methyl and methoxy compounds (Table 2). In fact, the substituent could be removed entirely with only a small effect on activity (31, Table 3). A wide range of groups were therefore introduced at this position to modulate the physicochemical properties. Compounds incorporating solubilizing groups were accessed via the phenol 32. As hoped, these analogues (e.g., 33, 34) had much improved solubility (Table 3) and retained most of the affinity of the simpler analogues, albeit with lower ligand efficiency.

SPR K_d Determination. To obtain label-free confirmation of binding to the BET bromodomains and an equilibrium binding constant, exemplars were tested in a surface plasmon resonance (SPR) assay. Compound 34 was found to have a K_d of 2–3 μM for BRD2 and BRD4 (Table 4), consistent with the micromolar TR-FRET IC_{50} values in Table 3.

Table 4. Surface Plasmon Resonance Binding Results Showing K_d for Compound 34 Binding to BRD2 and BRD4^a

BRD2		BRD4	
K_d (μM)	Rmax (RU)	K_d (μM)	Rmax (RU)
2.1	53	1.6	25
4.7	43	4.7	43
3.3	34	1.9	39
2.5	55		

^aAverage BRD2 K_d = 3.14 μM (SD 1.65); BRD4 K_d = 2.75 μM (SD 1.76).

Selectivity. Selectivity profiles of compounds were assessed by thermal melting (T_m) assays. These were performed against BET family single and tandem bromodomains as well as eight other proteins selected to sample other branches of the phylogenetic tree. ΔT_m results are shown in Figure 4 for compounds 6a and 34. Both compounds stabilized the melting temperature of the BET bromodomains consistently, most notably in the tandem BD12 constructs, where a shift of over 5 $^\circ\text{C}$ was observed in the case of BRD4. For the other bromodomains, the effects were much smaller (≤ 1.5 $^\circ\text{C}$), suggesting that there is a window of selectivity between the BET family and other bromodomains, although this method does not permit a precise quantitation.

Cellular Activity. BET inhibitors show potent effects in cellular systems, including inhibition of pro-inflammatory cytokine production.⁵ In an LPS-stimulated human PBMC assay, examples of the sulfonamide series inhibited IL-6 production at about the micromolar level (Tables 2, 3). In line with results from the BZD series,¹⁰ the IC_{50} s observed in the in vitro binding assays translated to very similar potencies in cellular readouts of cytokine reduction. The correlation between the BRD4 FA binding assay and the PBMC IL-6 assay is consistent with BET inhibition being the mode of action of the cellular efficacy (Figure 5, $r^2 = 0.57$). For comparison, the mean IC_{50} of 2 in the IL-6 assay is 400 nM, consistent with its greater binding assay potency.

Example sulfonamides were also tested for their ability to inhibit TNF α release from LPS-stimulated PBMCs. Compound 6a had an IC_{50} of ~ 200 nM in this assay ($\text{pIC}_{50} = 6.9$, mean of 8 values, standard deviation 0.56). The potency was reduced in an assay measuring the suppression of TNF α production in LPS-stimulated human whole blood (5 μM for 6a), probably reflecting the suboptimal physicochemical characteristics of this compound.

DISCUSSION

Inhibiting protein–protein interactions (PPIs) with small molecules is often perceived as challenging.^{12–14} Even when it is possible to find ligand-efficient starting points, the elaboration of these to yield biologically active compounds without compromising traditional drug-like properties can prove problematic. It has even been suggested that to increase the probability of success, Lipinski's rules for drug-likeness¹⁵ need to be relaxed and modified for molecules that target PPIs.¹⁶ However, while some targets are undeniably difficult, not all PPI interfaces are flat and featureless. In an accompanying manuscript, we reported the use of focused fragment screening to find diverse low-MW BET bromodomain inhibitors that bind at one "hotspot", the acetyl-lysine pocket.

One common difficulty in interpreting high concentration biochemical FBDD screening is in verifying that weak fragments interact directly with the target rather than interfere with the assay. This may be one reason why apparently promising hits can prove impossible to optimize. In this example, the hits were validated by orthogonal assays and X-ray crystallography, confirming both their binding mode and the underlying knowledge-based strategy used to drive the compound screening set selection.⁷

Starting from the isoxazole fragment hit, our knowledge of the BET family active site predicted that the WPF shelf would be an important region to enhance potency and selectivity. Analogues were selected to exploit this, leading to an immediate increase in potency of 2 orders of magnitude. Importantly, this was accompanied by structure–activity relationships which could be rationalized crystallographically. After available compounds had been screened, additional molecules were selected through modeling and synthesized to complete our evaluation. Members of the series achieve higher ligand efficiency than the BZD and related BET inhibitors discovered through phenotypic screening. SAR within the series is consistent with the crystallographic binding mode, and levels of cellular anti-inflammatory activity correlate with BET binding affinity. Furthermore, our assessment of selectivity suggests that, despite their relatively small size, members of this sulfonamide series bind to the BET family bromodomains preferentially over other bromodomains.

The resulting series binds using an isoxazole AcK-mimetic template unknown in the literature until very recent disclosures. This chemotype appears to have been found in several different ways, demonstrating the tractability of the BET family to a variety of lead discovery approaches. The first 3,5-dimethyl isoxazole BET inhibitors to be published belong to a related quinoline series.^{17,18} These were found through phenotypic screening and were optimized to high levels of potency and cellular efficacy without any knowledge of the molecular target.^{19,20}

After the first draft of this manuscript was submitted, a paper by Hewings et al. appeared online in this journal describing BET inhibitors also containing 3,5-dimethyl isoxazole as the acetyl-lysine mimic.²¹ The discovery was serendipitous, arising from screening analogues of a dihydroquinazolinone hit. In the crystal structure of the complex between BRD4-BD1 and the dihydroquinazolinone, the positioning of the dimethyl isoxazole group is very similar to that of 3 in BRD2-BD1 reported above. As with our work, optimization led to phenyl 3-substituted compounds, the most potent of which was compound 4d of Hewings et al. (35, Figure 6). The X-ray structure of 35 in

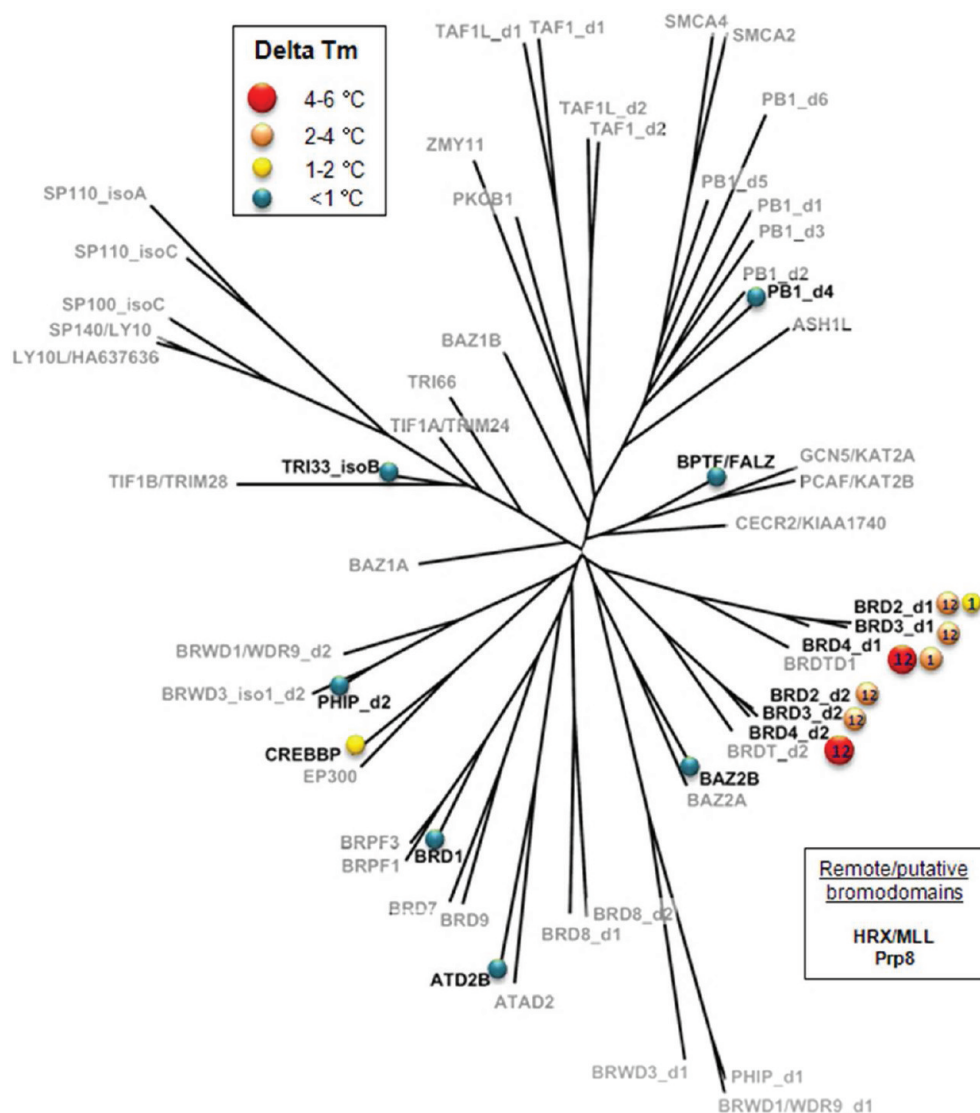


Figure 4. Bromodomain selectivity of representative compounds **6a** and **34** using a thermal shift assay. The average temperature shifts (T_m) in $^{\circ}\text{C}$ upon addition of $100\ \mu\text{M}$ compound are represented by color-coded spheres as indicated in the key. The thermal shift was virtually identical for these two molecules and so can be adequately represented by a single summary. The one exception is for the CREBBP domain, where compound **34** showed a $1.5\ ^{\circ}\text{C}$ shift and compound **6a** gave a $< 1\ ^{\circ}\text{C}$ shift. Bromodomains not assessed as part of the selectivity panel are shown in gray. Proteins were expressed as N-terminally His6 or His6-FLAG tagged constructs. Constructs comprising more than one bromodomain are designated as, e.g., BD12, denoting that the construct contains two bromodomains BD1 and BD2.

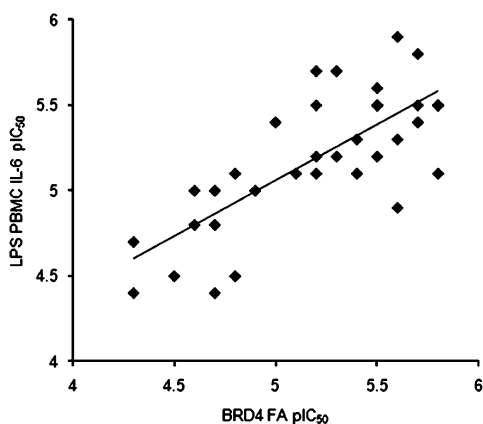


Figure 5. Correlation between 36 sulfonamides in the PBMC IL-6 assay and the BRD4 FA binding assay: $\text{pIC}_{50} = \log_{10} \text{IC}_{50}$ ($r^2 = 0.57$).

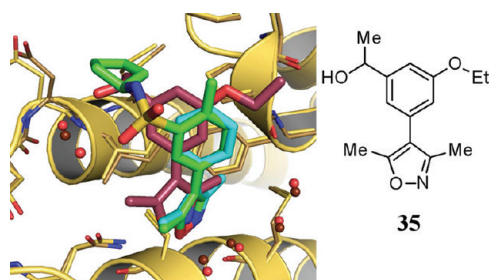


Figure 6. Comparison between the BRD2-BD1 crystal structure of **6a** (green, with BRD2 in yellow) superimposed on that of **3** (cyan). The BRD4-BD1 complex with **35** is also shown (deep red).²¹

BRD4 showed that the terminal methyl group of its (*R*)-configuration secondary alcohol occupies the WPF shelf. Unexpectedly, a comparison of this structure with our BRD2

complexes reveals that relative to the position of the fragment 3, the substituted phenyl isoxazole of 35 moves some distance from the acetyl lysine pocket toward the WPF shelf.²¹ When the protein backbones are superimposed, the rmsd between the phenyl 3,5-dimethyl isoxazole core of 35 and that of 3 is 1.5 Å (Figure 6). This movement toward the WPF shelf suggests that the secondary alcohol substituent of 35 may not be quite large enough and that a longer group might allow it to fulfill the WPF binding interaction while maintaining the optimal placement of the fragment 3 within the AcK site (as found for 6a).

It is difficult to say whether this structural difference is accompanied by a difference in potency because the IC₅₀ value (and thus ligand efficiencies) of 35 were measured with an AlphaScreen assay and are not directly comparable with ours. Hewings et al. reported IC₅₀s for 3 of 34 μM (BRD2) and 84 μM (BRD4), lower than the value of >200 μM measured in our FA assay. Relative to 3, the optimized secondary alcohol 35 is ~20-fold more potent, while the cyclopentyl sulfonamide 6a is over 100-fold more potent. Interestingly, Hewings et al. also reported that some dimethyl isoxazoles can bind to CREBBP, which could be consistent with the marginally significant T_m shift seen for 34 (Figure 4).

CONCLUSION

These are not the first bromodomain inhibitors reported, but for the first time we have demonstrated the process of X-ray structure-guided optimization of a bromodomain fragment into a series of drug-like molecules with anti-inflammatory activity. Crystallography has subsequently validated the predictions made during each step of the design process. We conclude that the BET bromodomains are highly tractable both to the FBDD approach to lead discovery and to structure-based rational optimization of the resulting fragments. Because of the amenability of the wider bromodomain target class to crystallographic studies, it is likely that similar approaches will be applicable to other members. The discovery that drug-like inhibitors of this histone reader module can be found in this way presents exciting new opportunities for targeted intervention spanning multiple disease areas.

EXPERIMENTAL SECTION

General Experimental. All solvents were purchased from Fisher Scientific Ltd. and commercially available reagents were used as received. All reactions were followed by TLC analysis (TLC plates GF254, Merck) or LCMS (liquid chromatography mass spectrometry) using a Waters ZQ instrument. All microwave reactions were carried out in a Biotage Initiator 60 focused beam microwave (400 W).

Purity of all compounds was determined by LCMS and ¹H NMR. NMR spectra were recorded on a Bruker AVANCE 400 spectrometer or a Bruker Ultrashield 400 MHz instrument. Abbreviations for multiplicities observed in NMR spectra: s, singlet; br s, broad singlet; d, doublet; t, triplet; q, quadruplet; p, pentuplet; spt, septuplet; m, multiplet. Column chromatography was performed on prepacked silica gel columns (30–90 mesh, IST) using a Biotage SP4. Mass spectra were recorded on a Waters ZQ (ESI-MS) spectrometer. The UPLC analysis was conducted on an Acquity UPLC BEH C18 column (50 mm × 2.1 mm, i.d. 1.7 μm packing diameter) at 40 °C. See Supporting Information for full details.

Synthetic Procedures. Compounds 5a–17a, 6b–15b, 20a, 22a, 25a, 26a, 28a, and 28b were purchased. Other compounds were prepared by one of two routes (Scheme 1). For route A, Suzuki coupling of 4-iodo-3,5-dimethyl isoxazole with the appropriate aryl boronic acid yielded 4-aryl 3,5-dimethyl isoxazoles. Treatment of these with chlorosulfonic acid and PCl₅ gave the desired sulfonyl chlorides

exclusively substituted *meta* to the dimethyl isoxazole. The sulfonamide products were obtained by addition of the amine under basic conditions with subsequent Boc deprotection with TFA where required. For route B, 3-bromosulfonamides were prepared from commercially available bromo-aryl sulfonyl chlorides and the appropriate amine. Suzuki coupling of these products with 3,5-dimethyl-4-(4,4,5,5-tetramethyl-1,3,2-dioxaborolan-2-yl) isoxazole afforded the isoxazole-aryl sulfonamides 5b, 6b, and 31. Further derivatization was achieved through alkylation of the phenol 32, formed via boron tribromide mediated demethylation of 6a, to yield the ethers 33 and 34. Alkylation of the sulfonamide nitrogen could be achieved through NaOH deprotonation and subsequent reaction with the appropriate alkyl halide to yield the tertiary sulfonamides 23b and 24b. See Supporting Information for full details.

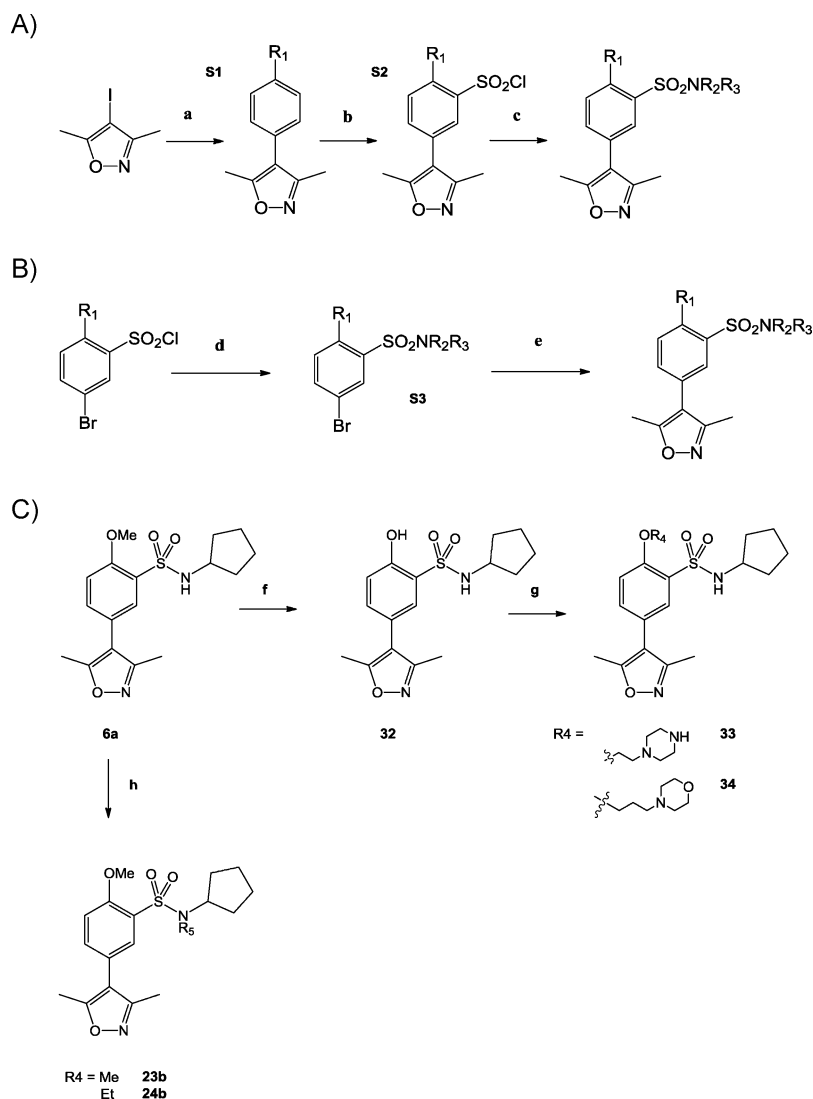
For example, 5b was prepared as follows. Cyclopropylamine (1.21 mL, 17.5 mmol), 5-bromo-2-methoxy benzene sulfonyl chloride (2.00 g, 7.0 mmol), and DIPEA (1.84 mL, 10.5 mmol) were combined as a solution in DCM (50 mL) and stirred at room temperature under N₂ overnight. The reaction mixture was washed with water (50 mL), dried, and concentrated in vacuo to yield crude desired product. Purification by flash column chromatography (silica gel, 7–100% ethyl acetate/cyclohexane) yielded 5-bromo-*N*-cyclopropyl-2-(methoxy)benzenesulfonamide S3a. S3a (1.94 g, 6.3 mmol), Pd(dppf)Cl₂ (463 mg, 0.63 mmol), and potassium carbonate (1.75 g, 12.7 mmol) were suspended in 1,4-dioxane (14 mL) and water (3.5 mL). The reaction mixture was heated at 100 °C for 45 min in a microwave reactor. The mixture was concentrated and ethyl acetate added (100 mL). The organics were washed with aqueous sodium carbonate solution (100 mL), dried, and concentrated to yield a brown residue. Purification by flash column chromatography (silica gel, 12–60% ethyl acetate/cyclohexane) yielded *N*-cyclopropyl-5-(3,5-dimethyl-4-isoxazolyl)-2-(methoxy) benzenesulfonamide 5b (1.38 g, 4.07 mmol, 64%) as a yellow solid. ¹H NMR (400 MHz, Chloroform-*d*) δ 7.88 (d, *J* = 2.5 Hz, 1H), 7.45 (dd, *J* = 2.5, 8.5 Hz, 1H), 7.14 (d, *J* = 8.5 Hz, 1H), 5.31 (s, 1H), 4.05 (s, 3H), 2.41 (s, 3H), 2.27 (s, 3H), 2.16 (m, 1H), 0.73 (m, 2H), 0.58 (m, 2H). LCMS: (ES+) 323, retention time 0.90 min, 97% pure.

Binding Assays and Fragment Screening. The tandem bromodomain constructs of BRD2, BRD3, and BRD4 were screened in two formats.¹⁰ The FA (fluorescence anisotropy) assay measures displacement of a labeled analogue of 1 and 2, while the TR-FRET (time-resolved fluorescence resonance energy transfer) assay measures displacement of a tetra-acetylated biotinylated peptide. The set of fragments was constructed and screened as previously described.⁷

IL-6 and TNF-α PBMC Assays. Peripheral blood mononuclear cells (PBMCs) purified from whole blood were incubated with LPS and varying concentrations of test compounds for 18–24 h. Inhibition of IL-6 or TNF-α was assessed as described in Supporting Information.

Surface Plasmon Resonance. Binding experiments with BRD4-BD12 and BRD2-BD12 were conducted at 25 °C on at least three occasions on a T200 BIAcore instrument. In all cases, a CMS chip with amine coupled protein was used. Flow cells of a CMS chip were first activated with 0.2 M *N*-ethyl-*N'*-(diethylaminopropyl)-carbodiimide (EDC) and 0.05 M *N*-hydroxysuccinimide (NHS). Typically 0.1–2 mg/mL BRD4-BD12/BRD2-BD12 at pH 4.5–5.5 in NaAc was then injected at 10 μL/min for 1–2 min, resulting in >5kRU of protein immobilized on the surface. The surface was neutralized with ethanolamine and extensively washed in the running buffer 50 mM HEPES pH7.5, 150 mM NaCl. Compounds were titrated as a tripling dilution starting at 10–20 μM. Sensorgrams and equilibrium binding curves were analyzed with BIAevaluation (GE Healthcare) using a 1:1 binding model. Parameters were derived from an equilibrium binding analysis. The equilibrium K_d was calculating using a 1:1 binding model, response = concentration × R_{max} / (Concentration + K_d) + offset.

Thermal Shift Assay (T_m). Thermal shifts of bromodomains marked in Figure 4 were analyzed on a Bioneer RT-PCR instrument. The temperature of the protein sample was ramped from 4 to 94 °C in

Scheme 1. Synthetic Routes^a

^a(A) R₁ = H or OMe. (a) R₁B(OH)₂, Pd(PPh₃)₄, Na₂CO₃ (aq), DME; (b) ClSO₃H, PCl₅, DCM; (c) (i) NHR₂R₃, NEt^tPr₂, DCM; (ii) TFA, DCM. (B) (d) NHR₂R₃, NEt^tPr₂, DCM; (e) Pd(dppf)Cl₂, K₂CO₃, 1,4-dioxane/water (4/1). (C) (f) BBr₃, DCM; (g) alcohol, PPh₃, DEAD, THF; (h) NaH, R₅-I, DMF. For full details, see Supporting Information.

the presence or absence of 100 μM of each compound in at least duplicate. Denaturation was visualized using 1:1000 dilution of a fluorescent Sypro orange dye in a buffer of PBS, 10% glycerol. The temperature was ramped at a rate of 1 °C/min and fluorescence readings taken every 0.5 °C. Bromodomains tested included ATAD2B, BAZ2B, BPTF, BRD1, BRD2 (bromodomain 1 and tandem), BRD3 (tandem), BRD4 (bromodomain 1 and tandem), CREBBP, PB1 (bromodomain 4), PHIP (bromodomain 2), and isoform B of TRIM33.

X-ray Crystallography. His-tagged BRD2-BD1 (67–200) was expressed in *E. coli*, purified, and crystallized. Compounds were soaked into apo crystals prior to crystal freezing and data collected as described in Supporting Information. Data collection and refinement statistics are given in Supporting Information Figure S1 and OMIT ($F_o - F_c$) maps in Figure 2.

Pharmacophore Design. The 3D pharmacophore model was constructed based on X-ray complexes of BRD2-BD1 with 1 and 3. Building on findings that structurally distinct inhibitors share common steric and electrostatic features at the bottom of the AcK-pocket,⁷ these were modeled using the structure of 3 bound into BRD2. To model the interaction with either the conserved asparagine Asn156 or the conserved water molecule near Tyr113, a hydrogen-bond acceptor pharmacophore feature was placed on the isoxazole nitrogen. A methyl

feature was placed upon the isoxazole 3-methyl to model the presence of a methyl group near Phe99. Another interaction with the lipophilic WPF shelf bordered by the WPF motif (BRD2 97–99), the “gatekeeper” Ile162, Met165, and Asp161 was modeled with a lipophilic feature near the centroid of the pendant phenyl ring of 2. Pharmacophore building and searching was carried out using MOE.²²

Quantum Mechanical Calculations. Gas phase quantum mechanical calculations were performed at the B3LYP/6-31G** level using Jaguar.²³

■ ASSOCIATED CONTENT

Supporting Information

Supplementary methods and chemistry; X-ray statistics; complete screening data. This material is available free of charge via the Internet at <http://pubs.acs.org>.

Accession Codes

Coordinates have been deposited with the Protein Data Bank (4a9m, 4a9n, 4a9o, 4a9p) and will be released immediately on publication.

AUTHOR INFORMATION

Corresponding Author

*Phone: +44 (0)20 8047 5000. Fax: +44 1438 763352. E-mail: Paula.Bamborough@gsk.com.

Author Contributions

^{||}These authors contributed equally to this work.

ACKNOWLEDGMENTS

We thank Stuart Baddeley, Matt Lindon, Peter Soden, Iain Uings, all other members of the bromodomain teams, the Apo-A1 team in GlaxoSmithKline, Les Ulis, Jason Witherington, Kevin Lee, and Epinova DPU, and the departments of Biological Reagents & Assay Development and Screening & Compound Profiling.

ABBREVIATIONS USED

AcK, acetyl-lysine (AcK); ApoA1, apolipoprotein A-1; ATAD2B, ATPase family AAA domain containing 2B; BAZ2B, bromodomain adjacent to zinc finger domain 2B; BET, bromodomain and extra-terminal; BD, bromodomain; BPTF, bromodomain PHD finger transcription factor; BRD1/2/3/4, bromodomain-containing protein 1/2/3/4; COX2, cyclooxygenase-2; CREBBP, cAMP response element-binding protein; HSQC, heteronuclear single-quantum correlation spectroscopy; IL-6, interleukin-6; LPS, lipopolysaccharide; NUT, nuclear protein in testis; PB1, polybromo 1; PCAF, P300/CBP-associated factor; PHIP, pleckstrin homology domain interacting protein; TRIM33, tripartite motif-containing 33; TR-FRET, time-resolved fluorescence resonance energy transfer

REFERENCES

(1) Sanchez, R.; Zhou, M. M. The role of human bromodomains in chromatin biology and gene transcription. *Curr. Opin. Drug Discovery Dev.* **2009**, *12*, 659–665.

(2) Denis, G. V. Bromodomain coactivators in cancer, obesity, type 2 diabetes, and inflammation. *Discoveries. Med.* **2010**, *10*, 489–499.

(3) Denis, G. V.; Nikolajczyk, B. S.; Schnitzler, G. R. An emerging role for bromodomain-containing proteins in chromatin regulation and transcriptional control of adipogenesis. *FEBS Lett.* **2010**, *584*, 3260–3268.

(4) Florence, B.; Faller, D. V. You bet-cha: a novel family of transcriptional regulators. *Front. Biosci.* **2001**, *6*, D1008–D1018.

(5) Nicodeme, E.; Jeffrey, K. L.; Schaefer, U.; Beinke, S.; Dewell, S.; Chung, C. W.; Chandwani, R.; Marazzi, I.; Wilson, P.; Coste, H.; White, J.; Kirilovsky, J.; Rice, C. M.; Lora, J. M.; Prinjha, R. K.; Lee, K.; Tarakhovskiy, A. Suppression of inflammation by a synthetic histone mimic. *Nature* **2010**, *468*, 1119–1123.

(6) Filippakopoulos, P.; Qi, J.; Picaud, S.; Shen, Y.; Smith, W. B.; Fedorov, O.; Morse, E. M.; Keates, T.; Hickman, T. T.; Felletar, I.; Philpott, M.; Munro, S.; McKeown, M. R.; Wang, Y.; Christie, A. L.; West, N.; Cameron, M. J.; Schwartz, B.; Heightman, T. D.; La, T. N.; French, C. A.; Wiest, O.; Kung, A. L.; Knapp, S.; Bradner, J. E. Selective inhibition of BET bromodomains. *Nature* **2010**, *468*, 1067–1073.

(7) Chung, C.; Dean, T.; Woolven, J.; Bamborough, P. Fragment-Based Discovery of Bromodomain Inhibitors Part 1: Inhibitor Binding Modes and Implications for Lead Discovery. *J. Med. Chem.* 10.1021/jm201320w.

(8) Schulz, M. N.; Hubbard, R. E. Recent progress in fragment-based lead discovery. *Curr. Opin. Pharmacol.* **2009**, *9*, 615–621.

(9) Hopkins, A. L.; Groom, C. R.; Alex, A. Ligand efficiency: a useful metric for lead selection. *Drug Discovery Today* **2004**, *9*, 430–431.

(10) Chung, C.; Coste, H.; White, J. H.; Mirguet, O.; Wilde, J.; Gosmini, R. L.; Delves, C.; Magny, S. M.; Woodward, R.; Hughes, S. A.; Boursier, E. V.; Flynn, H.; Bouillot, A. M.; Bamborough, P.; Brusq, J. M.; Gellibert, F. J.; Jones, E. J.; Riou, A. M.; Homes, P.; Martin, S. L.;

Uings, I. J.; Toum, J.; Clement, C. A.; Boullay, A. B.; Grimley, R. L.; Blandel, F. M.; Prinjha, R. K.; Lee, K.; Kirilovsky, J.; Nicodeme, E. Discovery and Characterization of Small Molecule Inhibitors of the BET Family Bromodomains. *J. Med. Chem.* **2011**, *54*, 3827–3838.

(11) The Structural Genomics Consortium. <http://www.thesgc.org>, 2011.

(12) Wells, J. A.; McClendon, C. L. Reaching for high-hanging fruit in drug discovery at protein-protein interfaces. *Nature* **2007**, *450*, 1001–1009.

(13) Dömling, A. Small molecular weight protein–protein interaction antagonists: an insurmountable challenge? *Curr. Opin. Chem. Biol.* **2008**, *12*, 281–291.

(14) Meireles, L. M.; Mustata, G. Discovery of modulators of protein–protein interactions: current approaches and limitations. *Curr. Top. Med. Chem.* **2011**, *11*, 248–257.

(15) Lipinski, C. A.; Lombardo, F.; Dominy, B. W.; Feeney, P. J. Experimental and computational approaches to estimate solubility and permeability in drug discovery and development settings. *Adv. Drug Delivery Rev.* **1997**, *23*, 3–25.

(16) Morelli, X.; Bourgeas, R.; Roche, P. Chemical and structural lessons from recent successes in protein–protein interaction inhibition (2P2I). *Curr. Opin. Chem. Biol.* **2011**, *15*, 475–481.

(17) Bouillot, A.-M.; Donche, F.; Gellibert, F.; Lamotte, Y.; Mirguet, O. Imidazo[4,5-c]quinoline derivatives as bromodomain inhibitors and their preparation and use in the treatment of cancer, chronic autoimmune and inflammatory disease. WO2011054846, 2011.

(18) Dawson, M. A.; Prinjha, R. K.; Dittmann, A.; Giotopoulos, G.; Bantscheff, M.; Chan, W. I.; Robson, S. C.; Chung, C. W.; Hopf, C.; Savitski, M. M.; Huthmacher, C.; Gudgin, E.; Lugo, D.; Beinke, S.; Chapman, T. D.; Roberts, E. J.; Soden, P. E.; Auger, K. R.; Mirguet, O.; Doehner, K.; Delwel, R.; Burnett, A. K.; Jeffrey, P.; Drewes, G.; Lee, K.; Huntly, B. J.; Kouzarides, T. Inhibition of BET recruitment to chromatin as an effective treatment for MLL-fusion leukaemia. *Nature* **2011**, *478*, 529–533.

(19) Mirguet, O.; Lamotte, Y.; Donche, F.; Toum, J.; Gellibert, F.; Bouillot, A.; Gosmini, R.; Nguyen, V. L.; Delannée, D.; Seal, J.; Blandel, F.; Boullay, A. B.; Boursier, E.; Martin, S.; Brusq, J. M.; Krysa, G.; Riou, A.; Tellier, R.; Costaz, A.; Huet, P.; Dudit, Y.; Trotter, L.; Nicodeme, E. From ApoA1 upregulation to BET family Bromodomain inhibition: Discovery of I-BET151 (GSK1210151A). Submitted for publication.

(20) Lamotte, Y.; Donche, F.; Bouillot, A.; Mirguet, O.; Gellibert, F.; Nicodeme, E.; Krysa, G.; Beinke, S.; McCleary, S.; Rioja, I.; Bamborough, P.; Chung, C.; Gordon, L.; Lewis, A.; Walker, A.; Cutler, L.; Lugo, J.; Seal, J. Identification of a novel series of BET family Bromodomain inhibitors: binding mode and profile of IBET-151 (GSK1210151A). Submitted for publication.

(21) Hewings, D. S.; Wang, M.; Philpott, M.; Fedorov, O.; Uttarkar, S.; Filippakopoulos, P.; Picaud, S.; Vuppusetty, C.; Marsden, B.; Knapp, S.; Conway, S.; Heightman, T. D. 3,5-Dimethylisoxazoles act as acetyl-lysine-mimetic bromodomain ligands. *J. Med. Chem.* **2011**, *54*, 6761–6770.

(22) *Molecular Operating Environment (MOE)*, version 2008.10; Chemical Computing Group (CCG), 2011.

(23) *Jaguar*, version 7.8; Schrodinger, LLC, New York, 2011.

(24) Moriniere, J.; Rousseaux, S.; Steuerwald, U.; Soler-Lopez, M.; Curtet, S.; Vitte, A. L.; Govin, J.; Gaucher, J.; Sadoul, K.; Hart, D. J.; Krijgsvelde, J.; Khochbin, S.; Muller, C. W.; Petosa, C. Cooperative binding of two acetylation marks on a histone tail by a single bromodomain. *Nature* **2009**, *461*, 664–668.